HHS Public Access

Author manuscript

J Nucl Med. Author manuscript; available in PMC 2015 July 01.

Published in final edited form as:

J Nucl Med. 2014 July ; 55(7): 1192–1197. doi:10.2967/jnumed.114.137448.

Comparison of the Hypoxia PET Tracer ^{18}F-EF5 to Immunohistochemical Marker EF5 in 3 Different Human Tumor Xenograft Models

Satish K. Chitneni[1], **Gerald T. Bida**[1], **Michael R. Zalutsky**[1,2], and **Mark W. Dewhirst**[2]

[1]Department of Radiology, Duke University Medical Center, Durham, North Carolina

[2]Department of Radiation Oncology, Duke University Medical Center, Durham, North Carolina

Abstract

The availability of ^{18}F-labeled and unlabeled 2-(2-nitro-1*H*-imidazol-1-yl)-*N*-(2,2,3,3,3-pentafluoropropyl)-acetamide (EF5) allows for a comparative assessment of tumor hypoxia by PET and immunohistochemistry; however, the combined use of these 2 approaches has not been fully assessed in vivo. The aim of this study was to evaluate ^{18}F-EF5 tumor uptake versus EF5 binding and hypoxia as determined from immunohistochemistry at both macroscopic and microregional levels.

Methods—Three tumor models— PC3, HCT116, and H460—were evaluated. Tumor-bearing animals were coinjected with ^{18}F-EF5 and EF5 (30 mg/kg), and PET imaging was performed at 2.5 h after injection. After PET imaging and 2 min after Hoechst 33342 injection, the tumors were excised and evaluated for ^{18}F-EF5 distribution by autoradiography and EF5 binding by immunohistochemistry. Additionally, the effects of nonradioactive EF5 (30 mg/kg) on the hypoxia-imaging characteristics of ^{18}F-EF5 were evaluated by comparing the PET data for H460 tumors with those from animals injected with ^{18}F-EF5 alone.

Results—The uptake of ^{18}F-EF5 in hypoxic tumor regions and the spatial relationship between ^{18}F-EF5 uptake and EF5 binding varied among tumors. H460 tumors showed higher tumor-to-muscle contrast in PET imaging; however, the distribution and uptake of the tracer was less specific for hypoxia in H460 than in HCT116 and PC3 tumors. Correlation analyses revealed that the highest spatial correlation between ^{18}F-EF5 uptake and EF5 binding was in PC3 tumors (r = 0.73 ± 0.02) followed by HCT116 (r = 0.60 ± 0.06) and H460 (r = 0.53 ± 0.10). Uptake and binding of ^{18}F-EF5 and EF5 correlated negatively with Hoechst 33342 perfusion marker distribution in the 3 tumor models. Image contrast and heterogeneous uptake of ^{18}F-EF5 in H460 tumors was significantly higher when the radiotracer was used alone versus in combination with unlabeled EF5 (tumor-to-muscle ratio of 2.51 ± 0.33 vs. 1.71 ± 0.17, P , 0.001).

For correspondence or reprints contact: Satish K. Chitneni, Box 3808, Department of Radiology, Duke University Medical Center, Durham, NC 27710. satish.chitneni@duke.edu..

DISCLOSURE

The costs of publication of this article were defrayed in part by the payment of page charges. Therefore, and solely to indicate this fact, this article is hereby marked “advertisement” in accordance with 18 USC section 1734. This work was supported by research grants from Varian Medical Systems and the NIH (CA40355, CA42324, and P41EB0015897). No other potential conflict of interest relevant to this article was reported.

Conclusion—The uptake and hypoxia selectivity of ^{18}F-EF5 varied among tumor models when animals also received nonradioactive EF5. Combined use of radioactive and nonradioactive EF5 for independent assessment of tumor hypoxia by PET and immunohistochemistry methods is promising; however, the EF5 drug concentrations that are required for immunohistochemistry assays may affect the uptake of ^{18}F-EF5 in hypoxic cells in certain tumor types as observed in H460 in this study.

Keywords

tumor; hypoxia; PET; ^{18}F-EF5; EF5

Hypoxia is a common feature of many solid cancers and has been shown to be an independent prognostic factor for disease progression in a variety of cancers (*1–3*). Hypoxia induces genomic changes, mostly mediated by the hypoxia-inducible factor family of transcription factors that lead to the upregulation of molecular pathways involving tumor angiogenesis and distant metastasis (*4*). Additionally, hypoxic tumor cells are less susceptible to the therapeutic effects of conventional radiation treatment and chemotherapy, thereby decreasing the sensitivity of hypoxic tumors to standard-of-care therapies (*5,6*). Hence, hypoxia has been recognized as an important target for cancer therapy, and several different treatment approaches are under evaluation for selective targeting of hypoxic cells or molecular pathways involving hypoxia (*7*). Hypoxia occurs with high heterogeneity within a tumor and between tumors of the same type, necessitating its measurement on an individual tumor basis for diagnosis and implementation of therapeutic strategies (*8,9*).

Though there are several imaging methods that are sensitive to oxygen concentration and for detecting hypoxic conditions in human tumors, PET is the leading technique because of its high sensitivity and the availability of several radiolabeled compounds as markers for tumor hypoxia (*10*). With the exception of ^{64}Cu-diacetyl-bis(N^4-methylthiosemicarbazone), current small-molecule PET hypoxia tracers consist of a 2-nitroimidazole moiety that forms the basis for their selective uptake in hypoxic tumor cells (partial pressure of oxygen < 10 mm Hg). 2-(2-nitro-1*H*-imidazol-1-yl)-*N*-(2,2,3,3,3-^{18}F-pentafluoropropyl)-acetamide (^{18}F-EF5) is a relatively new 2-nitroimidazole–based PET tracer that has shown a good safety profile and acceptable radiation dose in cancer patients (*11–13*). Moreover, its usefulness for imaging tumor hypoxia has been demonstrated in head and neck cancer and glioblastoma (*11,12*). In preclinical studies, hypoxia PET tracers are often coadministered with immunohistochemical markers such as pimonidazole and EF5 to validate PET data and to enable comparison of radiotracer uptake with the microregional distribution of hypoxia as measured by immunohistochemistry (*14,15*). In this regard, ^{18}F-EF5 offers a distinct advantage over other 2-nitroimidazole hypoxia tracers in that nonradioactive EF5 has been extensively validated as an immunohistochemistry marker for tumor hypoxia (*16–18*). Immunohistochemical measurement of high EF5 binding has been shown to be associated with a more aggressive phenotype in multiple cancers (*16–18*). However, there are no published studies that directly compare ^{18}F-EF5 versus EF5 immunohistochemistry or assess the effects of the high concentrations of EF5 required for immunohistochemistry on tumor uptake and distribution of ^{18}F-EF5 determined by PET. Such comparisons are needed to validate the combination for parallel measurement of hypoxia by PET and

immunohistochemistry. Herein, we have evaluated the tumor up-take and hypoxia selectivity of ^{18}F-EF5 when used in combination with immunohistochemistry doses of EF5 in 3 different tumor models. In animals receiving ^{18}F-EF5 plus EF5, the tumor uptake of the radiotracer was compared with EF5 binding and hypoxia at the whole-section level, and the spatial correlation between ^{18}F-EF5 uptake and EF5 binding was assessed.

MATERIALS AND METHODS

Radiotracer and Fluorescence Markers

The radiolabeling precursor, 2-(2-nitro-1[*H*]-imidazol-1-yl)-*N*-(2,3,3-trifluoroallyl)-acetamide, and the nonradioactive EF5 were provided by Varian Medical Systems. ^{18}F-EF5 was synthesized as previously described except that ^{18}F[F_2] was produced using a 6061 T6 aluminum target and the amount of radiolabeling precursor used in the study was 7 mg (28 μmol) (*19*). The specific activity of the radiotracer was 94.6 ± 22.5 MBq/μmol at the end of synthesis (n = 15). Hoechst 33342 was purchased from Sigma-Aldrich. The Cy5-conjugated anti-EF5 antibody, ELK3-51 Cy5 (75 μg/mL), was obtained from the University of Pennsylvania (Dr. Cameron Koch).

Tumor Models and PET Imaging

All animal experiments were conducted in accordance with a protocol approved by the Duke University Institutional Animal Care and Use Committee. Xenografts derived from 3 different tumor cell lines, human colorectal carcinoma (HCT116), prostate adenocarcinoma (PC3), and human non–small cell lung carcinoma (H460), were used in the study. HCT116 and PC3 xenografts were established by sub-cutaneous injection of 2×10^6 tumor cells suspended in 0.1 mL of culture medium and Matrigel (1:1; BD Biosciences) into the hind limb of athymic mice (NCr-*nu/nu*). H460 tumors were initiated by injecting 5×10^6 cells in 0.2 mL of culture medium and Matrigel (1:1) into the hind limb of athymic rats (NIH-RNU).

Imaging experiments were initiated when tumor volume reached at least 500 mm^3 for HCT116 and PC3 and 1,000 mm^3 for H460 (rats). PET imaging was performed by acquiring a 20-min static scan on a microPET R4 scanner (Siemens Medical Solutions) 2.5 h after the animals had been injected with a mixture of ^{18}F-EF5 and nonradio-active EF5 (EF5: 30 mg/kg of body weight; ^{18}F-EF5 specific activity, 9.8 ± 3.3 MBq/μmol [n = 9]). After imaging, the animals were injected with the perfusion marker Hoechst 33342, and 2 min later, tumors were excised and snap-frozen using liquid nitrogen. Frozen tumor tissue was then transferred to a cryostat for section cutting. The time difference between EF5 administration and tumor tissue collection was 180 ± 0.3 min (n = 10). PET data were reconstructed using 3-dimensional ordered-subsets expectation maximization plus maximum a posteriori algorithm with an image matrix of 128 × 128 × 63 and a pixel size of 0.85 mm. The reconstructed images were analyzed for tumor uptake of ^{18}F-EF5 by drawing 3-dimensional regions of interest over the entire tumor area using AMIDE software (amide.sf.net). Background activity levels were obtained from the muscle region of the contralateral leg for each animal. The images were corrected for radioactivity decay but not for attenuation and scatter. Standardized uptake values were recorded for all voxels within the tumor regions of interest, and the mean and maximal standardized uptake values were

calculated for each tumor. Additionally, for H460 tumors, the hypoxic tumor fraction was determined using a tumor-to-muscle (T/M) threshold of 1.5 for significant hypoxia (*11*).

Autoradiography and Immunofluorescence Imaging

For each tumor, a series of 12-μm sections was cut from 3 different levels ranging from the periphery to the mid-tumor level and exposed to storage phosphor screens at 4°C overnight. Digital autoradiography (DAR) images were developed by scanning the screens on a Cyclone Plus Phosphor Imager (Perkin Elmer), and the images were analyzed with OptiQuant software (Packard Instruments Co.). Tumor sections adjacent to those used for autoradiography were stored at −80°C and used for immunohistochemical staining with anti-EF5 antibody. Briefly, the frozen tumor sections were thawed and first imaged for Hoechst fluorescence to obtain in vivo perfusion maps. Next, the tumor sections were fixed in cold methanol and were blocked with donkey serum (Jackson Immunoresearch). Sections were treated with Cy5-conjugated anti-EF5 antibody (1:1 dilution in phosphate-buffered saline) at 4°C overnight and imaged using a scanning stage fluorescence microscope (Axioskop 2 Plus; Carl Zeiss) with the ×5 objective lens for a fixed exposure time.

Image Registration and Spatial Correlation Analysis

For each animal, 2 (H460) or 3 (HCT116 and PC3) pairs of tumor sections were compared section by section via ^{18}F-EF5 autoradiography and EF5 immunohistochemistry. The result was a comparison of 8–9 pairs of DAR and immunohistochemistry sections representing different tumor locations and underlying microenvironment conditions for each tumor model. First, the fluorescence images (EF5, Hoechst) were rescaled to match the image size and pixel size (42 μM) of the DAR image and subsequently coregistered in Photoshop CS5 (Adobe Systems). Visual landmarks such as tumor edges, marker uptake, and necrosis patterns were used as the basis for alignment of the image sets. Spatial correlation analysis was performed on the coregistered images using the colocalization plug-in in ImageJ software, and scatterplots were generated from these data for each set of autoradiography and fluorescence images with an effective pixel size of 126 mm (3 × 3 pixel binning). An automated threshold scheme built into the ImageJ program (modified IsoData) was used to apply thresholds to the images to determine the ^{18}F-EF5–positive uptake area fraction and the EF5 staining area fraction on whole tumor sections to enable comparison with the PET data and the spatial correlation analysis.

Data Analysis

Data are presented as mean ± SD. Statistical comparisons were made using t tests. Spatial correlation analysis was assessed using the Pearson correlation coefficient (r). Data were analyzed using Prism (version 5.01; GraphPad), and statistical significance was determined at a P level of less than 0.05.

RESULTS

^{18}F-EF5 Uptake Versus EF5 Binding and Hypoxia in 3 Tumor Models

Three tumor models—PC3, HCT116, and H460—were used to study the uptake and spatial distribution of ^{18}F-EF5 in relation to EF5 binding and hypoxia. Figure 1 shows examples of

small-animal PET images obtained at 2.5 h after injection of ^{18}F-EF5–plus–EF5 in the 3 tumor models, and the representative autoradiography and composite fluorescence images of tumor sections (EF5, green; Hoechst 33342, blue) obtained from these animals are shown in Figures 2–4. Scatterplots showing the spatial correlation between ^{18}F-EF5 tumor distribution and EF5 binding are also shown for the corresponding tumor sections in Figures 2–4. In PET imaging, H460 tumors showed the highest image contrast, with a mean T/M ratio of 1.76 ± 0.17 (n = 4) compared with 1.37 ± 0.18 for HCT116 (n = 3) and 1.18 ± 0.30 for PC3 (n = 3). The T/M ratios measured on PET images correlated significantly with those determined from ex vivo γ counting of tumor and muscle tissues (r = 0.78; P < 0.01; Supplemental Fig. 1 [supplemental materials are available at http://jnm.snmjournals.org]).

For H460 and HCT116 tumors, the average ^{18}F-EF5 uptake area fraction measured from autoradiography images was considerably higher than the hypoxic area fraction determined from the immunohistochemistry images, whereas for PC3 tumors, there was a close correspondence between the two, with an average ^{18}F-EF5–positive uptake area fraction of 0.36 ± 0.10 compared with an EF5 staining area fraction of 0.32 ± 0.06 (Table 1). Accordingly, visual comparison of the DAR and immunohistochemistry images revealed higher hypoxia-specific uptake of ^{18}F-EF5 in PC3 tumors (Fig. 2) than in HCT116 (Fig. 3) and H460 (Fig. 4) tumors. For HCT116 tumors, the uptake of ^{18}F-EF5 was grossly similar to the EF5 binding seen in immunohistochemistry images, and there was good contrast between radiotracer uptake in hypoxic and nonhypoxic tumor regions in DAR images (Fig. 3). However, H460 xenografts showed lower contrast in ^{18}F-EF5 uptake between hypoxic and nonhypoxic tumor regions (Fig. 4). The uptake or retention of the tracer in nonhypoxic tumor regions appeared to be higher in H460 xenografts than that seen in similar regions in HCT116 and H460 tumors. At the macroscopic level (whole-section), the ^{18}F-EF5–positive uptake area fraction (DAR) correlated positively with the hypoxic fraction determined by EF5 in immunohistochemistry images. Correlation between the 2 methods was higher in PC3 tumors (r = 0.95) than in HCT116 (r = 0.79) or H460 (r = 0.72) tumors (Fig. 5).

Spatial Correlation Between ^{18}F-EF5, EF5, and Hoechst 33342

The spatial correlation between uptake of ^{18}F-EF5, EF5, and Hoechst 33342 in tumors is shown in Table 1. In line with the macroscopic evaluation and visual comparisons (Figs. 2–4), correlation analysis revealed that the best spatial correlation between ^{18}F-EF5 uptake and EF5 binding was in PC3 tumors, with a somewhat lower correlation in HCT116 and H460 tumors. The average correlation coefficient was 0.73 ± 0.02 (slope, 0.99 ± 0.13) for PC3 tumors, compared with 0.60 ± 0.06 (slope, 0.66 ± 0.12) and 0.53 ± 0.10 (slope, 0.56 ± 0.13) for HCT116 and H460 tumors, respectively (Table 1). In all 3 models, uptake and binding of the hypoxia markers (^{18}F-EF5, EF5) negatively correlated with the per-fusion marker Hoechst 33342 (Table 1; Supplemental Fig. 2), and EF5 binding was minimal in tumor areas that were positive for Hoechst 33342 (Figs. 2B–4B). For H460 tumors, the negative relationship observed between nonradioactive EF5 binding and Hoechst was significantly higher than that for the ^{18}F-EF5–Hoechst combination (–0.23 ± 0.07 vs. –0.06 ± 0.07, P < 0.01), likely because of the clear absence of EF5 binding and the consequent low fluorescence signal in Hoechst-positive (perfused) tumor regions as opposed to the significant ^{18}F-activity retention seen in these regions in the DAR images. Similarly,

HCT116 tumors showed a significantly higher negative correlation for the 2 fluorescence markers than for ^{18}F-EF5 versus Hoechst (–0.17 ± 0.11 vs. –0.09 ± 0.11, $P < 0.001$). In contrast, no significant difference was observed between the correlation coefficients of EF5 versus Hoechst and ^{18}F-EF5 versus Hoechst in PC3 tumors (–0.16 ± 0.21 vs. –0.12 ± 0.21, $P = 0.21$), suggesting more hypoxia-specific binding and retention of the tracer in PC3 than in the other 2 tumors (Table 1; Figs. 2–4). Of note, the spatial correlation analysis for the 2 fluorescence markers EF5 and Hoechst 33342 was performed on the same tumor section, compared with adjacent sections for ^{18}F-EF5 versus Hoechst 33342.

^{18}F-EF5 With and Without EF5 in H460 Tumors

To further investigate the low spatial correlation observed between ^{18}F-EF5 uptake and EF5 binding in H460 tumors, comparisons were made between the imaging data of ^{18}F-EF5 plus EF5 versus ^{18}F-EF5 alone. Figure 6 shows the data from these experiments. The overall tumor uptake of the radiotracer and the image contrast were significantly higher when the animals were injected with ^{18}F-EF5 alone. The average tumor mean standardized uptake value for the ^{18}F-EF5–alone group was 0.70 ± 0.14, compared with 0.56 ± 0.10 for the ^{18}F-EF5–plus–EF5 group ($P = 0.08$). The maximum standardized uptake values and T/M ratios were significantly higher for the ^{18}F-EF5–alone animals than for animals that received the ^{18}F-EF5 and EF5 mixture (Fig. 6; $P < 0.01$ and $P < 0.001$, respectively). Similarly, the fraction of tumor voxels with T/M intensity ratios greater than 1.5 (hypoxic fraction threshold) was also significantly higher for the ^{18}F-EF5– alone group than for the ^{18}F-EF5–plus–EF5 group (0.92 ± 0.07 vs. 0.72 ± 0.15, $P < 0.05$). Comparison of DAR images of tumor sections from representative animals showed markedly higher tracer uptake and higher T/M signal intensities (≤4.3) in ^{18}F-EF5–alone animals than in EF5-coinjected animals (maximum T/M intensity, 2.8) (Supplemental Fig. 3).

DISCUSSION

In this study, we compared the PET tracer ^{18}F-EF5 in 3 different tumor models at a single time point and directly against its non-radioactive analog EF5, which is a thoroughly validated marker for tumor hypoxia by immunohistochemical methods. PC3, HCT116, and H460 tumor models were selected on the basis of previous studies demonstrating hypoxia in these xenografts with ^{18}F-EF5 by PET imaging or ex vivo γ counting (*19–21*). This study revealed that the uptake and the hypoxia selectivity of ^{18}F-EF5 vary with tumor type when used in conjunction with nonradioactive EF5 for immunohistochemistry staining (30 mg/kg). Of the 3 models, PC3 tumors showed the best spatial correlation and linear relationship between ^{18}F-EF5 uptake and EF5 binding in adjacent tumor sections ($r = 0.73 ± 0.02$; slope, 0.99 ± 0.13), followed by HCT116, which also showed a good correlation between the 2 hypoxia markers ($r = 0.60 ± 0.06$). In H460 tumors, the areas of high ^{18}F-EF5 uptake in DAR images corresponded to the areas of high EF5 binding in adjacent tumor sections; however, there was a significant retention of radioactivity in nonhypoxic tumor regions, resulting in poor contrast between hypoxic and nonhypoxic tumor regions and affecting the specificity of ^{18}F-EF5 uptake in this xenograft (Fig. 4). These results suggest differences in the specific uptake and clearance of unbound ^{18}F-EF5 in different tumor types when the radiotracer is coinjected with nonradioactive EF5.

Several studies have used EF5 immunohistochemistry for validation of PET hypoxia tracers and reported good spatial correlations between PET tracer uptake and EF5 binding in tumor xenografts. For example, Riedl et al. have shown a close correlation between ^{124}I-labeled iodoazomycin galactopyranoside uptake and EF5 in Morris hepatoma tumors, with a spatial correlation coefficient of 0.76 (22). Yuan et al. correlated the uptake of ^{64}Cu-diacetylbis(N^4-methylthiosemicarbazone) with EF5 binding in 3 different tumor lines and observed good spatial correlation between the 2 markers in R3230Ac tumors (r = 0.74) and 9L glioma (r = 0.61) but low correlation in fibrosarcoma tumors (r = 0.11), suggesting hypoxia-dependent uptake of ^{64}Cu-diacetyl-bis(N^4-methylthiosemicarbazone) in R3230Ac and 9L but not in fibrosarcoma (23). A few preclinical studies have also used the combined administration of ^{18}F-EF5 and EF5 for PET and immunohistochemical analysis of tumor hypoxia; however, none of the studies examined the spatial relationship between tumor binding of the 2 markers (^{18}F-EF5 and EF5) (*24–26*). In studies by Koch et al., the radiation response of 9L rat gliosarcoma tumors assessed by clonogenic assays (surviving fraction) correlated significantly with both tumor uptake of ^{18}F-EF5 (T/M or tumor-to-blood ratios) and EF5 binding; however, no correlation was found between the 2 hypoxia assays (^{18}F-EF5 uptake ratios vs. EF5 binding) at a whole-tumor level (*25*). Notably, 19 of 22 tumors in their study had T/M or tumor-to-blood ratios of less than 2 (Fig. 4 in the article by Koch et al. (*25*).). Although a different tumor type, H460 tumors in the current study, on rats, had T/M ratios of less than 2.0 (range, 1.5–1.9) when the animals were coinjected with nonradioactive EF5. In contrast, the T/M ratios in H460 tumor–bearing rats that did not receive unlabeled EF5 were all greater than 2.0 (range, 2.0– 3.0). Furthermore, comparison of autoradiography images and voxel-wise data from the representative animals from the 2 groups revealed a substantial decrease in hypoxia-specific uptake of the tracer in EF5-coinjected H460 tumor–bearing animals than in the ^{18}F-EF5–alone group (Fig. 4 and Supplemental Fig. 3). A similar discrepancy between tumor uptake of ^{18}F-EF5 and EF5 binding was reported in Shionogi tumors (*26*). Taken together, these data suggest that, in some tumor types, the unlabeled EF5 is affecting the uptake of ^{18}F-EF5 in hypoxic tumor cells or interfering with the clearance of unbound ^{18}F-EF5 from the tumor tissue, both of which could affect the hypoxia specificity of ^{18}F-EF5.

A recent study evaluating the radiation dosimetry and biodistribution of ^{18}F-EF5 found considerable differences in the absorbed radiation dose estimates for the excretory pathway organs urinary bladder and gallbladder at 2 different study sites (*13*). These differences were attributed to differences in ^{18}F-EF5 specific activity; the Turku group used a higher-specific-activity synthesis route, resulting in a lower EF5 concentration and faster elimination kinetics than seen in patients at the University of Pennsylvania (*13,21*). On the basis of literature data, the approximate plasma half-lives of ^{18}F-EF5 at drug concentrations (EF5) of 0.5 nM, 50 nM, and 50 μM in cancer patients are estimated to be 7.5, 10.5, and about 13.0 h, respectively (*12,13,27*), suggesting the influence of specific activity on the pharmacokinetic parameters of ^{18}F-labeled EF5. In our study, the addition of unlabeled EF5 to the radiotracer for immunohistochemistry purposes resulted in an approximately 10-fold reduction in the specific activity of ^{18}F-EF5 compared with the use of ^{18}F-EF5 alone, and the results from our study further suggest that specific activity may also influence the tumor distribution and

hypoxia selectivity of ^{18}F-EF5 in some tumor types as seen in the data from H460 tumor xenografts in this study.

CONCLUSION

The uptake and spatial distribution of ^{18}F-EF5 in relation to the well-established hypoxia marker EF5 was evaluated in PC3, HCT116, and H460 tumors. The hypoxia-specific uptake of ^{18}F-EF5 and its correlation with EF5 was highest in PC3, followed by HCT116 tumors, but was modest in H460 tumor xeno-grafts. Combined use of radioactive and nonradioactive EF5 for independent assessment of tumor hypoxia by PET and immunohistochemistry techniques is promising; however, unlabeled EF5 at doses commonly used for the immunohistochemistry assays (e.g., 30 mg/kg intravenously) can affect the hypoxia selectivity of ^{18}F-EF5 in some tumor types.

Supplementary Material

Refer to Web version on PubMed Central for supplementary material.

ACKNOWLEDGMENTS

We thank Shawn Murphy and Michael Dailey for assistance with $^{18}F_2$ production, and Dr. Hong Yuan (UNC–Chapel Hill) and Dr. Thies Schroeder for helpful discussions.

REFERENCES

1. Vaupel P, Schlenger K, Knoop C, Hockel M. Oxygenation of human tumors: evaluation of tissue oxygen distribution in breast cancers by computerized O_2 tension measurements. Cancer Res. 1991; 51:3316–3322. [PubMed: 2040005]
2. Brizel DM, Sibley GS, Prosnitz LR, Scher RL, Dewhirst MW. Tumor hypoxia adversely affects the prognosis of carcinoma of the head and neck. Int J Radiat Oncol Biol Phys. 1997; 38:285–289. [PubMed: 9226314]
3. Milosevic M, Warde P, Menard C, et al. Tumor hypoxia predicts biochemical failure following radiotherapy for clinically localized prostate cancer. Clin Cancer Res. 2012; 18:2108–2114. [PubMed: 22465832]
4. Semenza GL. Hypoxia-inducible factors: mediators of cancer progression and targets for cancer therapy. Trends Pharmacol Sci. 2012; 33:207–214. [PubMed: 22398146]
5. Trédan O, Galmarini CM, Patel K, Tannock IF. Drug resistance and the solid tumor microenvironment. J Natl Cancer Inst. 2007; 99:1441–1454. [PubMed: 17895480]
6. Dewhirst MW, Cao Y, Moeller B. Cycling hypoxia and free radicals regulate angiogenesis and radiotherapy response. Nat Rev Cancer. 2008; 8:425–437. [PubMed: 18500244]
7. Wilson WR, Hay MP. Targeting hypoxia in cancer therapy. Nat Rev Cancer. 2011; 11:393–410. [PubMed: 21606941]
8. Evans SM, Hahn SM, Magarelli DP, Koch CJ. Hypoxic heterogeneity in human tumors: EF5 binding, vasculature, necrosis, and proliferation. Am J Clin Oncol. 2001; 24:467–472. [PubMed: 11586098]
9. Vaupel P, Hockel M, Mayer A. Detection and characterization of tumor hypoxia using pO_2 histography. Antioxid Redox Signal. 2007; 9:1221–1235. [PubMed: 17536958]
10. Chitneni SK, Palmer GM, Zalutsky MR, Dewhirst MW. Molecular imaging of hypoxia. J Nucl Med. 2011; 52:165–168. [PubMed: 21233176]
11. Komar G, Seppaenen M, Eskola O, et al. ^{18}F-EF5: a new PET tracer for imaging hypoxia in head and neck cancer. J Nucl Med. 2008; 49:1944–1951. [PubMed: 18997048]

12. Koch CJ, Scheuermann JS, Divgi C, et al. Biodistribution and dosimetry of ^{18}F-EF5 in cancer patients with preliminary comparison of ^{18}F-EF5 uptake versus EF5 binding in human glioblastoma. Eur J Nucl Med Mol Imaging. 2010; 37:2048–2059. [PubMed: 20585774]
13. Lin LL, Silvoniemi A, Stubbs JB, et al. Radiation dosimetry and biodistribution of the hypoxia tracer ^{18}F-EF5 in oncologic patients. Cancer Biother Radio-pharm. 2012; 27:412–419.
14. Troost EGC, Laverman P, Kaanders JHAM, et al. Imaging hypoxia after oxygenation-modification: comparing ^{18}F-FMISO autoradiography with pimonidazole immunohistochemistry in human xenograft tumors. Radiother Oncol. 2006; 80:157–164. [PubMed: 16905213]
15. Oehler C, O'Donoghue JA, Russell J, et al. ^{18}F-fluromisonidazole PET imaging as a biomarker for the response to 5,6-dimethylxanthenone-4-acetic acid in colorectal xenograft tumors. J Nucl Med. 2011; 52:437–444. [PubMed: 21321262]
16. Evans SM, Judy KD, Dunphy I, et al. Comparative measurements of hypoxia in human brain tumors using needle electrodes and EF5 binding. Cancer Res. 2004; 64:1886–1892. [PubMed: 14996753]
17. Evans SM, Fraker D, Hahn SM, et al. EF5 binding and clinical outcome in human soft tissue sarcomas. Int J Radiat Oncol Biol Phys. 2006; 64:922–927. [PubMed: 16458778]
18. Evans SM, Du KL, Chalian AA, et al. Patterns and levels of hypoxia in head and neck squamous cell carcinomas and their relationship to patient outcome. Int J Radiat Oncol Biol Phys. 2007; 69:1024–1031. [PubMed: 17967299]
19. Chitneni SK, Bida GT, Dewhirst MW, Zalutsky MR. A simplified synthesis of the hypoxia imaging agent 2-(2-nitro-1H-imidazol-1-yl)-N-(2,2,3,3,3-^{18}F-pentafluoropropyl)-acetamide (^{18}F-EF5). Nucl Med Biol. 2012; 39:1012–1018. [PubMed: 22727821]
20. Chitneni SK, Bida GT, Yuan H, et al. ^{18}F-EF5 PET imaging as an early response biomarker for the hypoxia-activated prodrug SN30000 combined with radiation treatment in a non-small cell lung cancer xenograft model. J Nucl Med. 2013; 54:1339–1346. [PubMed: 23740105]
21. Eskola O, Gronroos TJ, Forsback S, et al. Tracer level electrophilic synthesis and pharmacokinetics of the hypoxia tracer ^{18}F-EF5. Mol Imaging Biol. 2012; 14:205–212. [PubMed: 21448777]
22. Riedl CC, Brader P, Zanzonico PB, et al. Imaging hypoxia in orthotopic rat liver tumors with iodine ^{124}I–labeled iodoazomycin galactopyranoside PET. Radiology. 2008; 248:561–570. [PubMed: 18641253]
23. Yuan H, Schroeder T, Bowsher JE, Hedlund LW, Wong T, Dewhirst MW. Inter-tumoral differences in hypoxia selectivity of the PET imaging agent ^{64}Cu(II)-diacetylbis(N4-methylthiosemicarbazone). J Nucl Med. 2006; 47:989–998. [PubMed: 16741309]
24. Ziemer LS, Evans SM, Kachur A, et al. Noninvasive imaging of tumor hypoxia in rats using the 2-nitroimidazole ^{18}F-EF5. Eur J Nucl Med Mol Imaging. 2003; 30:259–266. [PubMed: 12552344]
25. Koch CJ, Shuman AL, Jenkins WT, et al. The radiation response of cells from 9L gliosarcoma tumours is correlated with ^{18}F-EF5 uptake. Int J Radiat Biol. 2009; 85:1137–1147. [PubMed: 19995239]
26. Yapp DTT, Woo J, Kartono A, et al. Non-invasive evaluation of tumour hypoxia in the Shionogi tumour model for prostate cancer with ^{18}F-EF5 and positron emission tomography. BJU Int. 2007; 99:1154–1160. [PubMed: 17309552]
27. Koch CJ, Hahn SM, Rockwell K, Covey JM, McKenna WG, Evans SM. Pharmacokinetics of EF5 2-(2-nitro-1-H-imidazol-1-yl)-N-(2,2,3,3,3-pentafluoropropyl) acetamide in human patients: implications for hypoxia measurements in vivo by 2-nitroimidazoles. Cancer Chemother Pharmacol. 2001; 48:177–187. [PubMed: 11592338]

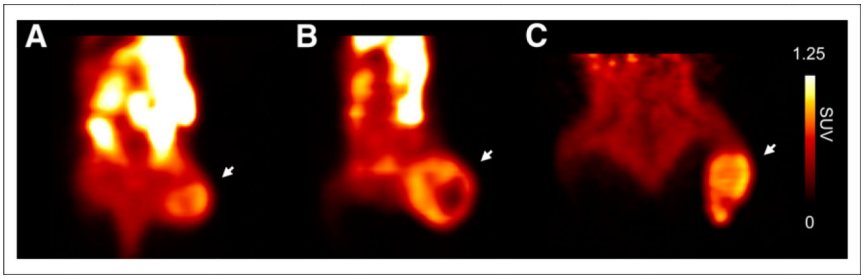

FIGURE 1.

^{18}F-EF5 PET images of PC3 (A), HCT116 (B) and H460 (C) tumor xenografts at 2.5 h after radiotracer injection. Images are scaled to same maximal standardized uptake value (SUV), and mid-coronal sections are shown for each of 3 tumors (indicated by arrows).

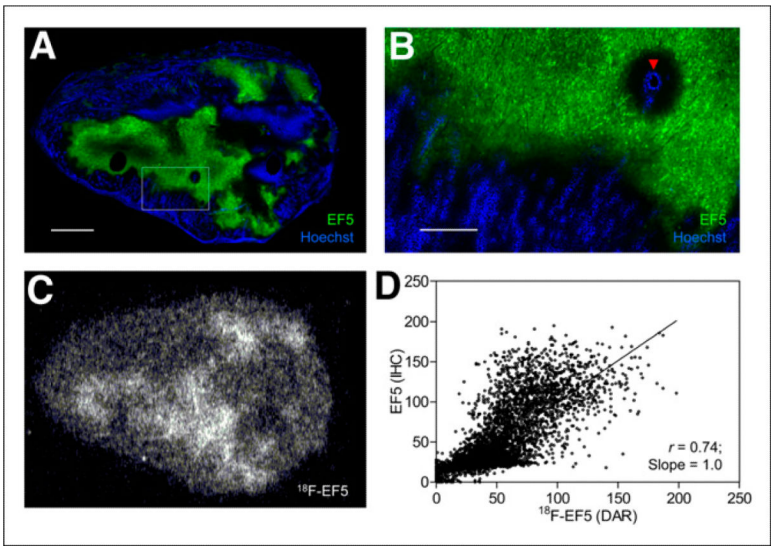

FIGURE 2.

Comparison of ^{18}F-EF5 uptake with EF5 binding and hypoxia in PC3 tumor model. (A) Composite fluorescence image showing EF5 binding in green and in vivo perfusion marked by Hoechst 33342 in blue. Scale bar = 2 mm. (B) High magnification of area shown in box on image A. Arrowhead indicates blood vessel. Scale bar = 0.5 mm. (C) Autoradiography image showing ^{18}F-EF5 uptake distribution in tumor section adjacent to that shown in A. (D) Spatial correlation analysis showing close correlation between EF5 binding and ^{18}F-EF5 uptake in tumor sections A and C (r = 0.74). Each point in scatterplot represents 126-μm pixel and corresponding marker values on coregistered image (immunohistochemistry and DAR).

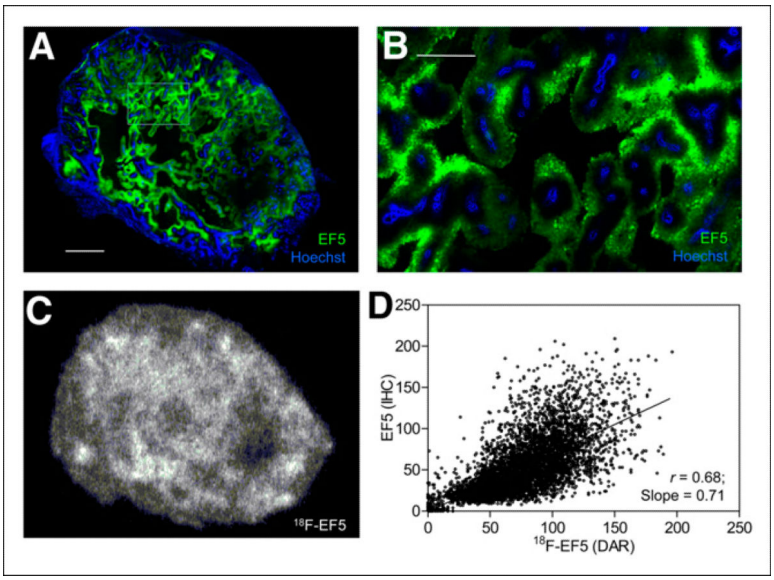

FIGURE 3.

^{18}F-EF5 uptake and hypoxia in HCT116 tumor. (A) Composite fluorescence images of EF5 and Hoechst 33342 for representative tumor section from animal shown in Figure 1B. Scale bar = 2 mm. (B) High magnification of area shown in box in image A. Scale bar = 0.5 mm. (C) Autoradiography image showing intratumoral distribution of ^{18}F-EF5 uptake. (D) Scatterplot showing spatial relationship between the 2 hypoxia markers on adjacent tumor sections shown in A and C.

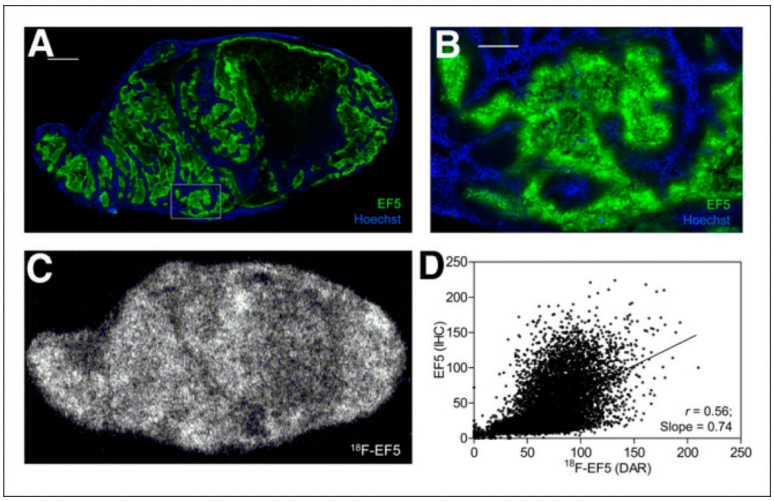

FIGURE 4.

Uptake and spatial distribution of ^{18}F-EF5 compared with EF5 binding in H460 tumor. Representative immunofluorescence (A) and autoradiography (C) images showing EF5 binding (green), vascular per-fusion (blue) and ^{18}F-EF5 distribution (C) in tumor xenograft shown in Figure 1C. Tumor area in box on image A is shown at high magnification in B. Spatial relationship between EF5 binding and ^{18}F-EF5 distribution determined from successive tumor sections in images A and C is shown in D. Scale bar in A = 2 mm and in B = 0.5 mm.

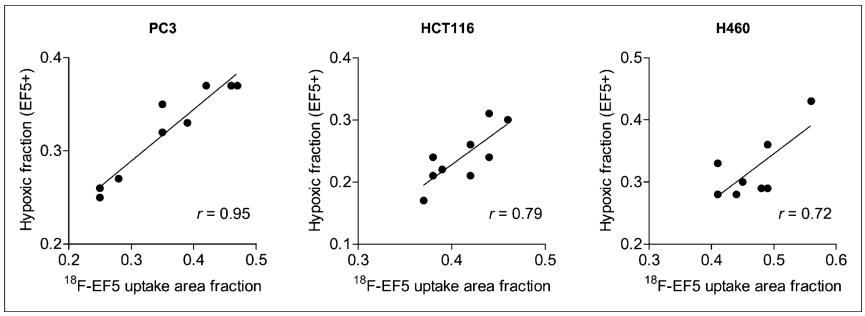

FIGURE 5.

Correlation of ^{18}F-EF5 uptake–positive area fraction with EF5 binding area fraction determined from adjacent tumor sections from same animal for each of 3 tumors.

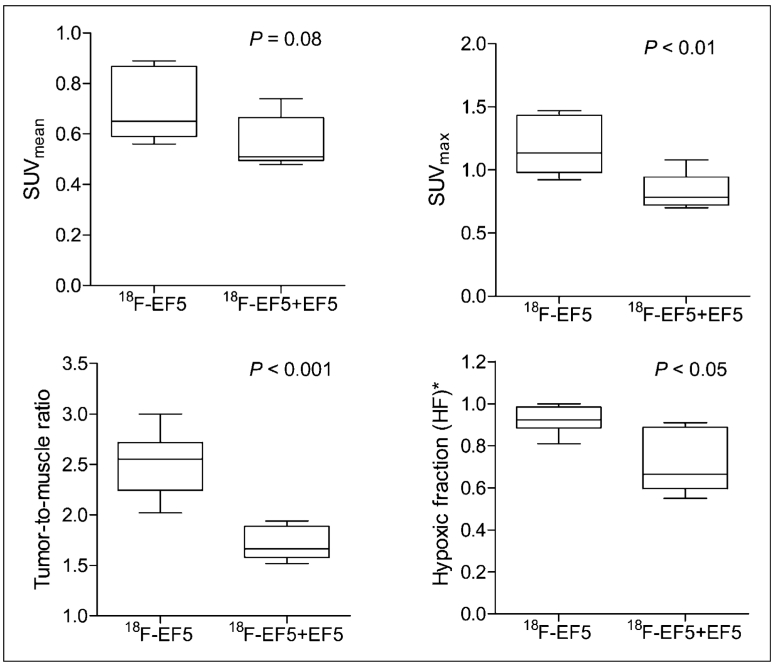

FIGURE 6.

Comparison of PET data for H460 tumor xenografts injected with ^{18}F-EF5 alone or mixture of ^{18}F-EF5 and EF5 (n = 6 animals per group). Line in box shows median value for group. *Fraction of voxels with T/M ratio > 1.5.

TABLE 1

Comparison of ^{18}F-EF5 Uptake with EF5 Binding and Hypoxia in 3 Tumor Models

Tumor type	^{18}F-EF5 uptake area fraction (DAR)	EF5 staining area fraction (immunohistochemistry)	Spatial correlation			
			^{18}F-EF5 vs. EF5		^{18}F-EF5 vs. Hoechst	
			r	Slope	*r*	Slope
PC3 (*n* = 3)	0.36 ± 0.10	0.32 ± 0.06	0.73 ± 0.02	0.99 ± 0.13	−0.12 ± 0.21	−0.10 ± 0.13
HCT116 (*n* = 3)	0.41 ± 0.03	0.24 ± 0.04	0.60 ± 0.06	0.66 ± 0.12	−0.09 ± 0.11	−0.04 ± 0.02
H460 (*n* = 4)	0.47 ± 0.05	0.32 ± 0.05	0.53 ± 0.10	0.56 ± 0.13	−0.06 ± 0.07	−0.02 ± 0.04